Korean J. Chem. Eng., 39(12), 3204-3213 (2022)
DOI: 10.1007/s11814-022-1297-7

pISSN: 0256-1115
eISSN: 1975-7220

Process modeling of syngas conversion to ethanol and acetic acid via the production of dimethyl ether and its carbonylation

Seungwoo Kim*, Hyun Seung Jung, Won Bo Lee*,†, Jong Wook Bae**,†, and Myung-June Park***,****,†**

*School of Chemical and Biological Engineering, Seoul National University, Seoul 08826, Korea
**School of Chemical Engineering, Sungkyunkwan University (SKKU), Suwon 16419, Korea
***Department of Chemical Engineering, Ajou University, Suwon 16499, Korea
****Department of Energy Systems Research, Ajou University, Suwon 16499, Korea
(*Received 14 April 2022 • Revised 23 August 2022 • Accepted 15 September 2022*)

Abstract−A process model was developed to simulate the generation of ethanol or acetic acid by selectively using syngas from coke oven gas as the carbon source. The simulation involved three reactors: the first reactor converts syngas into dimethyl ether over a hybrid Cu/ZnO/Al_2O_3/ferrierite catalyst; in the second reactor, carbonylation of dimethyl ether to methyl acetate takes place. The kinetic parameters for the carbonylation reaction were estimated by fitting the model to the experimental results. The third reactor uses the hydrogenation or hydrolysis of the methyl acetate to selectively synthesize ethanol or acetic acid, respectively. In the integrated process, a recycling loop was introduced, and its effects on the conversion, carbon molar yield, energy consumption, and capital and utility costs were evaluated. The results show that the recycling loop could enhance the carbon molar yield by approximately 20 times compared to that in the open-loop case owing to the high overall conversion (91-97%) of dimethyl ether in the second reactor.

Keywords: Carbonylation of Dimethyl Ether, Methyl Acetate, Kinetic Parameter Estimation, Process Modeling and Optimization

INTRODUCTION

In the past few decades, the reduction in fossil fuel sources and growing concern about environmental problems have generated the need for more research into alternatives to petroleum-derived fuels [1-3]. Ethanol is considered an important alternative synthetic fuel for automotive engines, chemical feedstocks, and hydrogen carriers [4-7]. Although biomass fermentation and ethylene hydration, two traditional pathways for ethanol production, have been commercialized, they have some limitations, such as the use of nonrenewable oil as the raw material and limited production capacity [8,9].

Acetic acid is also an essential product that is used as a food preservative, a solvent, or an intermediate for various products. For example, acetic acid is a key source of vinyl acetate monomer and acetic anhydride; it can also be an effective solvent for the production of purified terephthalic acid, for which the demand is increasing, especially in Southeast Asia. Conventionally, the oxidation of ethylene and hydrocarbons has been the main synthetic route for acetic acid [10]. Recently, a fermentative process for the production of acetic acid using carbon sources via environment-friendly pathways has been proposed [11]. However, significant amounts of byproducts, such as acetaldehyde and formic acid, make it difficult to separate acetic acid from the product in the conventional process. In recent production routes, scale-up is still limited, which motivates an economic analysis using process simulation based on kinetic models.

Methyl acetate (MA) can be a useful intermediate for the production of ethanol and acetic acid because of its uncomplicated synthesis pathways. The hydrogenation and hydrolysis of MA yield ethanol and acetic acid, respectively, and many studies have been conducted to develop suitable catalysts and kinetics. Cu/CeO_2 and Cu/SiO_2 core-shell catalysts have been fabricated using a facile sol-gel method that showed outstanding activity and stability in the hydrogenation of MA [12,13]. Furthermore, the activity of Cu/ZnO catalysts for MA hydrogenation can be enhanced by adding a MgO promoter to the catalyst [14]. Methanol, another product of MA hydrogenation, can be easily separated by a variety of methods, such as the use of a porous coordination polymer, pervaporation via a membrane, or distillation with an ionic liquid [15-17]. In the case of the hydrolysis of MA to obtain acetic acid, kinetic expressions have been investigated, with the parameters fitted to a large database for both homogeneous and heterogeneous reactions of MA [18]. Adsorption equilibrium constants, dispersion coefficients, and kinetic parameters have been obtained for the hydrolysis of MA over Amberlyst 15 ion-exchange resin [19].

Carbonylation of dimethyl ether (DME) has been considered a main synthetic route for MA, and many studies have been conducted to increase its efficiency [4,20,21]. However, some traditional carbonylation catalysts have disadvantages, such as a short catalyst lifetime, high cost, and environmental problems [22-24]. To overcome these issues, DME carbonylation over a ferrierite (FER) zeolite catalyst was considered in this study, and a kinetic model was developed based on experimental data under various operating con-

†To whom correspondence should be addressed.
E-mail: wblee@snu.ac.kr, finejw@skku.edu, mjpark@ajou.ac.kr

ditions. The kinetic model developed is integrated into a reactor module in a process simulator. After the MA from the DME carbonylation is separated, it can be either utilized directly or subjected to hydrogenation or hydrolysis to obtain ethanol or acetic acid. The synthesis of MA from syngas via DME has rarely been proposed in previous research, with no suggestion of industrial applications. Therefore, after the proposed process model for producing ethanol and acetic acid from syngas via DME and MA was shown to be valid, it was optimized to enhance the efficiency of the process. Finally, cost analysis was conducted to compare the capital and energy costs of all the cases considered in the present study.

MATERIALS AND METHODS

1. Catalyst for DME Carbonylation

1-1. Catalyst Preparation

The seed-derived FER zeolite catalyst was prepared using a hydrothermal synthesis method. A synthesis gel was prepared from fumed silica (Sigma Aldrich), sodium aluminate (Sigma Aldrich), and commercial NH_4-form FER (Zeolyst; Si/Al ratio ~10) as the seed materials. First, a basic solution was prepared by mixing NaOH and deionized water (DIW), followed by the addition of the fumed silica and, after a 1-h interval, the commercial FER seed. After the addition of the FER seed, the solution was vigorously stirred for 11 h, and then sodium aluminate was added to the mixture, which was stirred for a further 12 h. The resulting synthesis gel had a molar ratio of fumed silica/sodium aluminate/DIW/NaOH equal to 1/0.096/36/0.15 and contained 7 wt% of seed FER. The synthesis gel was transferred to an autoclave with a Teflon liner and subjected to hydrothermal synthesis at 160 °C for 96 h with tumbling. The product was washed with DIW, dried at 80 °C in an oven, and calcined at 550 °C (ramping at 1 °C/min) for 6 h to produce Na-form FER. The Na-form FER was added to 1 M ammonium nitrate solution (to a concentration of 1 g FER per 100 mL ammonium nitrate solution) and stirred at 80 °C for 3 h to allow ion exchange to occur. The ion exchange was repeated six times to ensure complete removal of Na ions, followed by calcination at 550 °C (ramping at 1 °C/min) for 3 h to prepare H-form of seed-derived FER, which was denoted as CFER-S1 7%.

1-2. Catalyst Characterization

The crystal structure of the synthesized seed-derived CFER-S1 7% was analyzed by X-ray diffraction (Bruker D8 Advance X-ray diffractometer) at 40 kV and 100 mA using Cu Kα radiation (λ= 0.15406 nm) and scanning at 4 degree/min over the range 2θ=5-50°. Peaks characteristic of the FER framework appeared at 9.3° and 12.8°.

1-3. Configuration of Fixed-bed Reactor for MA Synthesis

A 4 g sample of the H-form seed-derived CFER-S1 7% catalyst was loaded into a SUS fixed-bed reactor with an inner diameter of 7 mm. The catalyst was pretreated at 500°C and atmospheric pressure for 1 h using pure N_2 gas with a gas hourly space velocity (GHSV) of 2,000 L/(kg_{cat}·h). After the pretreatment, DME carbonylation was performed under various reaction conditions in the ranges 180-240 °C, 5-20 bar, and 2,000-6,000 L/(kg_{cat}·h) using gas mixtures of DME/CO/N_2 in the ratios 5/45/50 and 4.5/90/5.5. The effluent gas was injected into a gas chromatograph (GC; YL6100, Young Lin Instrument Co.) equipped with a flame ionization detector and a DB-wax capillary column.

Kinetic data were obtained at various operating temperatures, pressures, GHSV, and CO/DME ratios. The detailed experimental conditions are listed in Table 1.

Based on the GC results for each entry, the values of DME conversion (X_{DME}) and product selectivity (S_{MA} and S_{MeOH}) were calculated using the following relations:

$$X_{DME} = \frac{n_{CH_4} + n_{MA} + n_{MEOH}}{n_{CH_4} + n_{MA} + n_{MEOH} + n_{DME}} \times 100 \quad \text{[C-mol\%]} \tag{1}$$

$$S_{MA} = \frac{n_{MA}}{n_{CH_4} + n_{MA} + n_{MeOH}} \times 100 \quad \text{[C-mol\%]} \tag{2}$$

$$S_{MeOH} = \frac{n_{MeOH}}{n_{CH_4} + n_{MA} + n_{MeOH}} \times 100 \quad \text{[C-mol\%]} \tag{3}$$

where n_i represents the number of moles of carbon present in the form of species *i*.

2. Kinetic Modeling

2-1. DME Carbonylation to Produce MA

The overall reaction mechanism for DME carbonylation ($CH_3OCH_3+CO \leftrightarrow CH_3COOCH_3$) is illustrated in Fig. 1.

In the first step (cf. Induction period in Fig. 1), DME reacts with Brønsted sites to form surface methyl groups and water. The coverage of methyl groups continues to build up until a steady-state is reached (when the catalyst is fully methylated). In the steady-state,

Table 1. Operating conditions for DME carbonylation in this work

Entry	Pressure [bar]	Temperature [°C]	GHSV [L/(kg_{cat}·h)]	CO/DME ratio	DME/CO/N_2 [%]
1	10	180	2,000	9	5/45/50
2	10	200	2,000	9	5/45/50
3	10	220	2,000	9	5/45/50
4	10	240	2,000	9	5/45/50
5	5	220	2,000	9	5/45/50
6	15	220	2,000	9	5/45/50
7	20	220	2,000	9	5/45/50
8	10	220	2,000	20	4.5/90/5.5
9	10	220	4,000	9	5/45/50
10	10	220	6,000	9	5/45/50

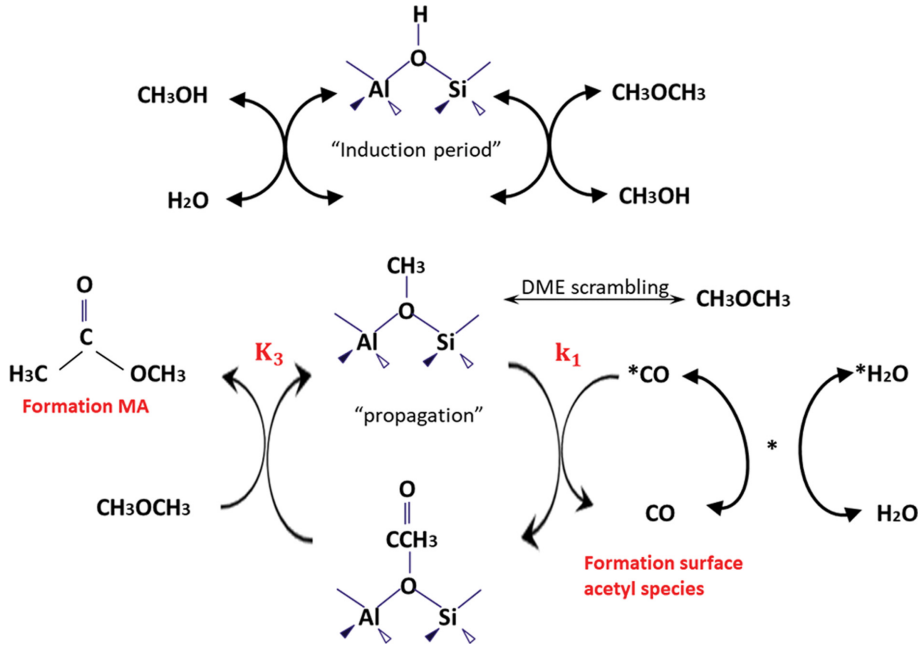

Fig. 1. Reaction pathways for DME carbonylation to synthesize MA over a FER catalyst [25].

CO reacts with methyl groups to produce surface acetyl species, followed by its reaction with DME to form MA and regenerate methyl groups [25-27]. Since 100% catalyst activity was assumed in this work, the side reaction in which MA blocks a methyl group during a quasi-equilibrium reaction, producing an inactive C[SiO(CH_3)Al] complex, was neglected, and the reaction of CO with a methyl group was considered an irreversible reaction.

Based on the above reaction mechanism, the reaction rate r_{MA} for MA synthesis was calculated as follows:

$$r_{MA}=\frac{k_1 P_{CO}}{\left(1+\frac{P_{MA}}{K_3\times P_{DME}}\right)} \quad (4)$$

where k_1 and K_3 represent the forward reaction rate constant for the formation of the surface acetyl species and the adsorption equilibrium constant, respectively.

2-2. Direct Synthesis of DME from Syngas over a Hybrid Catalyst

In our previous study [28], a kinetic model for the direct synthesis of DME from syngas over a hybrid Cu/ZnO/Al_2O_3 (CZA/FER) catalyst was developed. Experimental data were fitted to estimate the kinetic parameters, whose validity was corroborated by comparison with the reported values for conventional catalysts. Based on the estimated activation energy of the CO_2 and CO hydrogenations, Eqs. (5) and (6) are the rate-determining steps in the overall reactions, plausibly resulting from the core-shell structure of the hybrid catalyst. The hybrid catalyst could achieve almost 100% conversion of CO by instantly converting the produced methanol to DME, while the two separate reactions (methanol production by hydrogenation of CO_2 and CO over CZA, and methanol dehydration to DME over FER) led to CO conversion being limited by the equilibrium. The direct synthesis of DME from syngas over a hybrid catalyst could also allow the number of separators to be reduced compared to conventional multiple-step-based DME synthesis, thereby saving energy and equipment costs. In this study, the same kinetic rate equations and parameters were used for the first reactor in which syngas is directly converted into DME. The reaction rate equations are summarized in the Supplementary Material (Eqs. (S1)-(S4)), and the values of the kinetic parameters can be found in an earlier report [28].

CO_2 hydrogenation: $CO_2+3H_2\leftrightarrow CH_3OH+H_2O$ (5)

CO hydrogenation: $CO+2H_2\leftrightarrow CH_3OH$ (6)

Reverse water-gas-shift: $CO_2+H_2\leftrightarrow H_2O+CO$ (7)

DME synthesis: $2CH_3OH\leftrightarrow CH_3OCH_3+H_2O$ (8)

2-3. Reactor Model and Kinetic Parameter Estimation

To evaluate the contribution of external mass diffusion, the dimensionless Mears parameter was calculated, based on the physical properties and experimental data. The value obtained was lower than the threshold of 0.15, and external mass diffusion was, therefore, neglected [29]. The limitation due to internal pore diffusion was also estimated based on the Weisz-Prater criterion [30]; according to this concept, a concentration gradient will exist if the value of the dimensionless Weisz-Prater parameter (C_{wp}) is much greater than unity. As the C_{wp} values were close to one under all experimental conditions in this study, the internal diffusion limitation was also disregarded. As a result, the following mass and energy balances were used to simulate the reactor dynamics:

Mass balance: $-u_s\frac{dC_i}{dz}+\rho_B\sum_{j=1}^{NR}r_{i,j}=0$ (9)

Energy balance: $\rho_g u_s C_p\frac{dT}{dz}=\rho_B\sum_{j=1}^{NR}(-\Delta H)r_j+\frac{4U}{D_t}(T_w-T)$ (10)

Boundary conditions: At z=0, $C_i=C_{i,in}$ and $T=T_{in}$ (11)

Under the operating conditions in this work, the calculated equilibrium conversions were 100%, whereas the observed values were below 40% (Fig. S1 in the Supplementary Material), indicating that the reactions were in the kinetic regime; accordingly, kinetic data were used in the kinetic parameter estimation.

The kinetic parameters were estimated by minimizing the objective function F_{obj} (the sum of the squares of the errors in the objective elements X, Eq. (12)). To estimate the parameters of the DME carbonylation reaction rates, the amount of DME conversion to MA was considered an objective element, and the estimation was performed using the "lsqcurvefit" subroutine in MATLAB (MathWorks, Inc.), in which the Levenberg-Marquardt method is applied.

$$F_{obj}=\sum_{j=1}^{NE}\left[\sum_i w_i\left(\frac{X_{i,\,cal}-X_{i,\,exp}}{X_{i,\,exp}}\right)^2\right] \quad (12)$$

In Eq. (12), NE is the number of experiments, and w_i is the weighting factors.

3. Integrated Process Modeling from Syngas to Ethanol and Acetic acid

Fig. 2 shows a schematic of the overall process that comprises three reactors and three feed flows. The syngas in Feed 1 is supplied to reactor 1 (R1) to be converted into DME. The composition of syngas was specified to be 21.88 mol% CO, 9.37 mol% CO_2, and 68.75 mol% H_2, assuming that it is available as a byproduct from coke oven gas (COG). This composition corresponds to the stoichiometric H_2 concentration, that is, the molar ratio $H_2/(2CO+3CO_2)$ is 0.96 for CO_x hydrogenation [31], which can be referred to Eqs. (5) and (6). DME is separated from the effluent of reactor 1 (R1) and then fed to reactor 2 (R2) along with Feed 2, which consists of pure CO. DME carbonylation takes place in R2, and the effects of the CO/DME ratio on the carbonylation rate are evaluated by changing the flow rate of Feed 2. Reactor 3 (R3) is used to produce ethanol or acetic acid by the hydrogenation or hydrolysis of MA, respectively; Feed 3 consists of pure hydrogen (H_2) or water (H_2O) for the production of ethanol or acetic acid, respectively. While Fig. 2(a) is an open-loop process with no recycle stream, Fig. 2(b) introduces a recycle loop to fully consume unreacted CO resulting from its supply in excess over DME. The effluent from R2 in the open-loop process contains more than 50 mol% of CO because the CO/DME ratio needs to be much greater than one to perform carbonylation sufficiently. Therefore, MA is separated from the effluent of R2 to feed R3, and the gas stream (containing unreacted CO) is recycled to achieve a higher yield in the overall process.

To model R1, the kinetic model described in Section 2.2.2. [28] was implemented in the kinetic reactor module of a process simulator. The temperature and pressure were set to 250 °C and 50 bar, respectively, and the space velocity was fixed at approximately 2,000 L/(kg_{cat}·h) for all cases. The kinetic model for DME carbonylation developed in this study was used in R2, and the CO/DME ratio was varied from 10 to 30 to evaluate its effects on the DME conversion and MA yield for the process and determine its optimal value. The model for R3 assumed the equilibrium condition because of the fast reaction rates of both the hydrogenation and hydrolysis of MA. The overall reactions for R3 are as follows.

$$\text{MA hydrogenation: } CH_3COOCH_3+2H_2\leftrightarrow C_2H_5OH+CH_3OH \quad (13)$$

$$\text{MA hydrolysis: } CH_3COOCH_3+H_2O\leftrightarrow CH_3COOH+CH_3OH \quad (14)$$

4. Estimation of Capital and Utility Costs

For all the cases in the study, capital and utility costs were compared to evaluate the economic efficiency of the process. First, the equipment cost was estimated based on the cost correlation functions in the literature [32] and the six-tenth rule was applied when their size exceeded the reported range of cost correlations [33]. Second, the utility cost was estimated, including electricity, cooling water, and natural gas. Electricity was consumed in a cryogenic distillation process and a compressor. Cooling water and natural gas were used to maintain the operating temperature of reactors, distillation columns, and a heater. Details of energy consumption in the utility streams are summarized in Table S1 (Supplementary Material). Assumptions of purchased equipment cost correlations and utility costs are listed in Table 2.

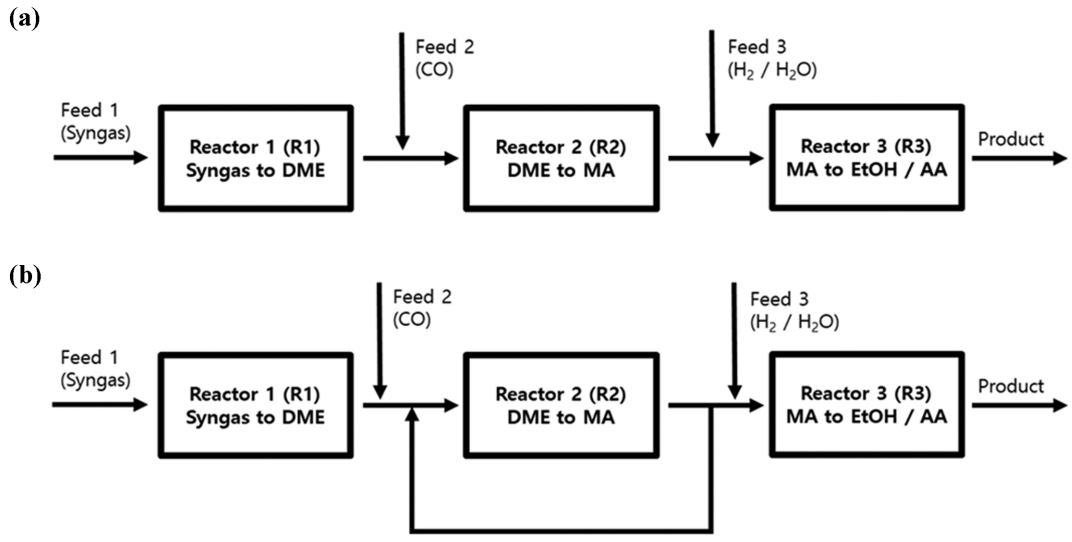

Fig. 2. Schematic of the overall process in the present study: (a) open-loop and (b) recycle-loop process.

Table 2. Correlations for the purchased costs and assumptions for utility costs

Equipment	Purchased cost [$]	Reference
Heat Exchangers, Reactors (R1, R2)	$C_p=\left(\frac{M\&S}{280}\right)(101.3A^{0.65}(F_d+F_p)F_m)$ $200<A<5{,}000\ ft^2$, Shell – and Tube type	[32]
Gas Compressor	$C_p=\left(\frac{M\&S}{280}\right)(517.5)(bhp)^{0.82}F_d$ $30<bhp<10{,}000$	
Distillation Columns, Reactors (R3)	$C_p=\left(\frac{M\&S}{280}\right)(101.9D^{1.066}H^{0.82}F_mF_p)$	
Utility	**Assumptions**	**Reference**
Cooling water	0.0148 $/ton	[34]
Electricity	0.06 $/kWh	
Natural gas	11.43 $/MWh	

C_p: purchased equipment cost [$], M&S: Marshall & Shift index, F_d: design parameter, F_p: pressure parameter, F_m: material parameter, A: area, bhp: brake horsepower, D: diameter [ft], H: tray stack height [ft]

Table 3. Estimated kinetic parameters

Parameter	Value	Unit
A_1	1.96	mol/(s·kg_{cat}·Pa)
$E_{a,1}$	84,040	J/mol
K_3	0.03	-

RESULTS AND DISCUSSION

1. Results of Parameter Estimation

Table 3 shows the estimated kinetic parameters, and Fig. 3 compares the experimental DME conversion data with the values calculated using the estimated parameters. The corresponding statistical parameters—the mean of the absolute relative errors (MARR) and the relative standard deviation of individual errors (RSDE)—were calculated to be 14.75% and 8.21%, respectively, indicating that the model developed in this work satisfactorily describes the experimental behavior of DME carbonylation.

Note that mordenite (MOR) catalyst was reported to be more active than FER for the DME carbonylation process [35]. However, although the MOR showed an initially high DME conversion, it was deactivated in a very short-term reaction period as confirmed

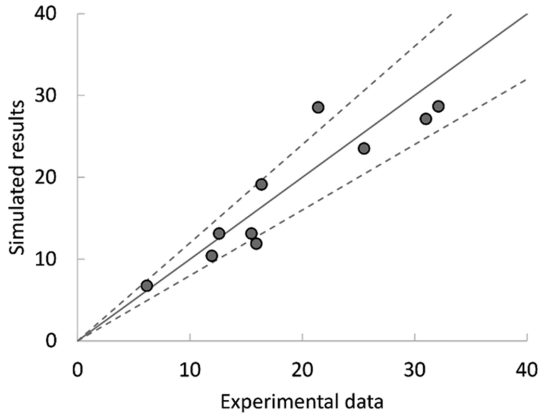

Fig. 3. Parity plot of DME conversion between experimental data and simulated results. The mean of the absolute relative errors (MARR) and the relative standard deviation of individual errors (RSDE) are 14.75% and 8.21%, respectively.

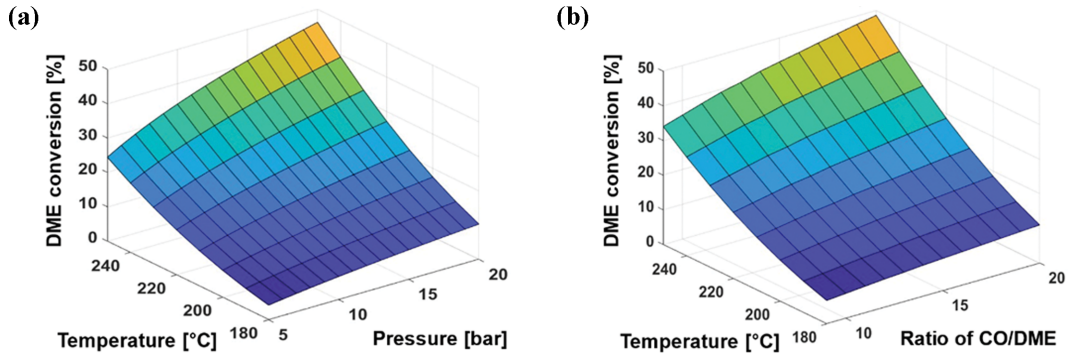

Fig. 4. Effects of (a) temperature and pressure and (b) temperature and the CO/DME ratio on DME conversion. The space velocity was fixed at 2,000 L/(kg_{cat}·h).

by our previous work [36], while FER zeolite after recrystallization was found to be much more stable than MOR. Therefore, process simulation was conducted based on the optimized FER.

Fig. 4 shows the effects of operating conditions on DME conversion. The conversions were calculated using the estimated kinetic parameters and the range of operating conditions were specified based on the experiments: CO/DME ratio of 9-20, pressure of 5-20, and temperature of 180-250 °C. The excess amount of CO made DME the limiting reactant; thus, the higher the ratio, the greater the DME conversion. Meanwhile, an increase in the total pressure increased the partial pressures of both CO and DME, resulting in an increased DME consumption rate, a feature that has been reported in the literature [25-27]. Because of the irreversibility of the reaction, that is, the absence of a thermodynamic limit, the reaction showed positive dependence on temperature.

2. Integrated Process Modeling and Cost Analysis

2-1. Integrated Process Modeling

Fig. 5 shows the process model for the production of ethanol and acetic acid from syngas in the Unisim Design Suite (Honeywell Inc.) in which the NRTL-SRK thermodynamic model was applied. The first distillation column (COL1) separates a liquid mixture of methanol and H_2O at 30 bar, and the compounds at the top of the column are fed to R2, which is operated at 20 bar and 220 °C. DME is the main product in R1, as well as the main feed in R2, while CO_2 and H_2 act as inert gases in R2. The flow rate of Feed2 (CO) was determined to satisfy the pre-specified value of the CO/DME ratio in R2. The condenser temperature was 16 °C, which indicated that cryogenic distillation was not required. The second column (COL2) represents the refluxed absorber module in the simulator (not a distillation column because MA was easily separated without the need for a reboiler after compressing the inlet stream to 27 bar) and achieves more than 99% recovery of MA. However, the condenser temperature was determined to be less than −20 °C, indicating that cryogenic distillation may be essential.

When a recycle loop was added to the MA synthesis reactor (Fig. 5(b)), DME was completely separated by an additional distillation column (COL3) to prevent inert gases, including CO_2, H_2, methanol, and H_2O, from accumulating in the recycled loop and thus increasing the required size of the reactor excessively. Pure (99 mol%) DME was fed into R2, and because of this high purity, only a 0.1% purge was considered necessary, corresponding to the almost complete recirculation of unreacted CO. The stoichiometric amount of CO was determined by Feed2 (CO), while an excessive amount of CO circulated in the recycle loop. More than 93 wt% purity of MA was achieved in the MA product stream, which was fed to R3, along with Feed3, which supplied H_2 (to produce ethanol) or H_2O (to produce acetic acid). The equilibrium reactor was assumed in R3 to achieve more than 95% conversion of MA, and the annual production rate was calculated based on 8000 operational hours per year. In both the open-loop and recycle-loop cases, the CO/DME ratio was varied from 10 to 30 to elucidate its effect on the conversion, carbon molar yield, and annual production rate. Although a high CO/DME ratio can boost productivity, too high a ratio might result in a large separation cost for the recovery of CO (COL2 condenser duty); thus, 30 was specified as the upper limit of the operating window.

A total of six cases were considered; Cases 1-3 and 4-6 correspond to the open-loop and recycle-loop cases, respectively, while different CO/DME ratios (10, 20, and 30) were considered in reactor R2. Detailed specifications are listed in Table 4. The same specifications and operating conditions were considered for the DME synthesis (R1). The reaction reached equilibrium, resulting in 95% consumption of CO and 31% production of CO_2 by the water-gas-shift reaction. This indicates that part of the CO was converted into CO_2 (not the full conversion of CO to DME), corresponding to a low carbon molar yield.

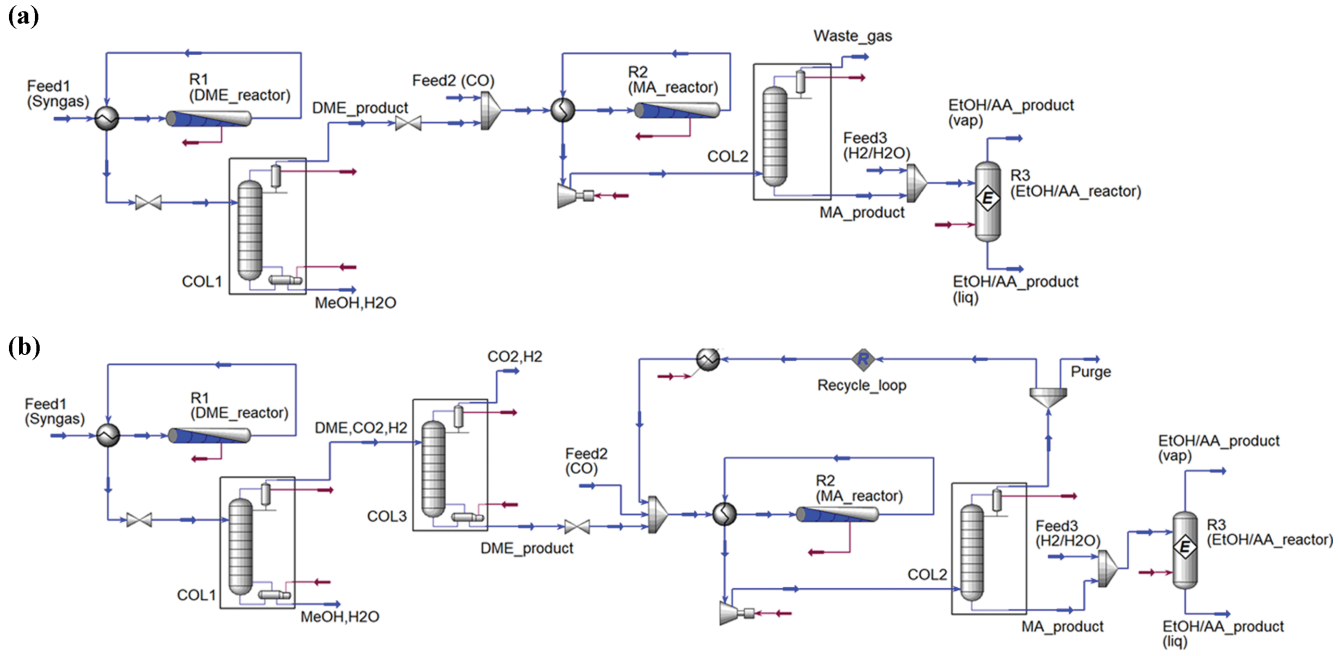

Fig. 5. (a) Open-loop and (b) recycle-loop process models for the production of ethanol/acetic acid via MA synthesis.

Table 4. Summarized results for the cases in this work

R1	Feed1 mass flow rate [kg/h]	88,340					
	Space velocity [L/kg_{cat}/h]	2,000					
	T (wall) [°C]	250					
	P [bar]	50					
	Conversion [%]	CO 95.03; CO_2 −31.39					
		Open-loop			**Recycle-loop**		
		Case 1	**Case 2**	**Case 3**	**Case 4**	**Case 5**	**Case 6**
R2	Feed2 mass flow rate [kg/h]	170,200	342,900	515,400	16,580	17,650	18,260
	Ratio of CO/DME at the inlet	**10**	**20**	**30**	**10**	**20**	**30**
	Space velocity [L/kg_{cat}/h]	2,004	2,007	2,001	2,009	1,997	2,013
	T (wall) [°C]	220	220	220	220	220	220
	P [bar]	20	20	20	20	20	20
	Waste gas mass flow rate [kg/h]	234,300	402,400	571,700	616.5	889.2	1,137
	Mass fraction of CO in waste gas (Open-loop) or purge (Recycle-loop) [%]	71.56	84.12	89.17	89.44	95.14	97.03
	DME Conversion [%][a]	27.71	38.24	45.58	27.88 (local); 91.26 (overall)	38.43 (local); 95.85 (overall)	45.34 (local); 97.43 (overall)
	COL2 condenser duty [MJ/h]	70,560	115,400	160,400	147,100	221,800	279,800
	Carbon molar yield [%][b]	4.02	3.2	2.68	65.42	67.23	67.52
	Annual production (MA) [ton/y]	100,560	138,630	165,050	332,820	349,620	355,500
R3 (Ethanol)	Feed3 mass flowrate [kg/h]	3,421	4,716	5,615	11,320	11,890	12,090
	H_2/MA	10	10	10	10	10	10
	MA Conversion [%]	98.88	98.88	98.89	98.89	98.89	98.89
	Carbon molar yield [%]	2.65	2.11	1.77	43.13	44.33	43.42
	Annual production [ton/y]	61,832	85,248	101,496	204,696	213,440	218,664
R3 (Acetic acid)	Feed3 mass flowrate [kg/h]	61,140	84,270	100,300	202,300	212,600	216,200
	H_2O/MA	20	20	20	20	20	20
	MA Conversion [%]	97.24	97.06	97.02	96.91	96.92	96.93
	Carbon molar yield [%]	2.08	2.07	1.73	42.27	43.44	43.71
	Annual production [ton/y]	79,392	109,027	129,800	261,456	274,688	279,368

[a]Local conversion was calculated using the reactor inlet and outlet streams, whereas the overall conversion was based on the feed and product streams.

[b]Carbon molar yield was defined as the number of moles×carbon number (moles) in the product divided by the total carbon moles in Feeds 1 and 2.

The mass flow rate of Feed2 (CO) was controlled to meet the specified value of the CO/DME ratio, and the DME conversion in R2 increased in both the open-loop and recycled cases. However, in the open-loop cases, the mass flow rate of waste gas and the mass fraction of CO in the waste gas also increased proportionally, indicating some waste of pure CO, as shown by the very low values of the carbon molar yield. Although DME conversion ranged between 27.71% and 45.57%, corresponding to the annual production of 100,000 to 165,000 tons/y, the yield of the overall process was significantly low (lower than 5%) because of the substantial amount of waste gas emitted after separating MA in COL2. Therefore, the recycle loop for R2 was included in Cases 4-6 to suppress waste gas emission and enhance the process yield.

Because nearly pure DME was fed to R2 by separating the inert gas in COL3, excessive CO was continuously circulated in the recycle loop, whereas Feed2 (CO) contained the stoichiometric amount of pure CO, as shown in the mass flow rate of Feed2 in Table 4. Although the local levels of DME conversion, which were calculated using the reactor inlet (feed+recycled stream) and the reactor effluent, were similar in the open and recycled cases for the

same CO/DME ratio, the overall DME conversion, which is based on the feed and product streams, reached nearly 100% for all the recycled cases, and the waste gas mass flow rate decreased by less than 0.5% compared to the open-loop cases. This increase in overall DME conversion resulted in a substantial increase in the carbon molar yield, which was more than 15 times higher than that in Cases 1-3, and the annual production of MA increased by more than 100% compared to the open-loop cases.

Feed 3 (H_2/H_2O) contains excessive H_2 or H_2O to ensure the productivity and carbon molar yield in the process when the MA has been almost completely converted. Despite the high MA conversion of close to 100%, the carbon molar yield is reduced by approximately two-thirds from the value in R2 because methanol is produced in both the hydrolysis and hydrogenation of MA. As shown in the detailed results in Table 4 for the open- and recycle-loop processes, the introduction of the recycle loop is essential to convert the carbon sources effectively and attain a high carbon molar yield. Although the increase in the CO/DME ratio in R2 slightly enhanced the annual production of ethanol and acetic acid, the cost of separating unreacted CO in COL2 also increased, resulting in a tradeoff between the annual production rate and the separation cost. In particular, as the condenser in COL2 operates at a temperature between −20 °C and −40 °C, the separation cost will be high, assuming cryogenic distillation. The COL2 condenser duty in Table 4 increases linearly with the CO/DME ratio. Based on this, the optimal CO/DME ratio was determined to be between 10 and 30, depending on the objective of the process.

2-2. Cost Analysis

Capital and operating costs were compared for all the cases. Fig. 6 shows the purchase cost of equipment and operating utility costs calculated based on the correlations and assumptions in Table 2. The energy consumption of each case, which was a key factor for calculating operating costs, is provided in Table S1 (Supplementary Material).

The heater was not included in Cases 1 to 3 (Open-loop), while the recycle-loop cases (Cases 4 to 6) included it to elevate the tem-

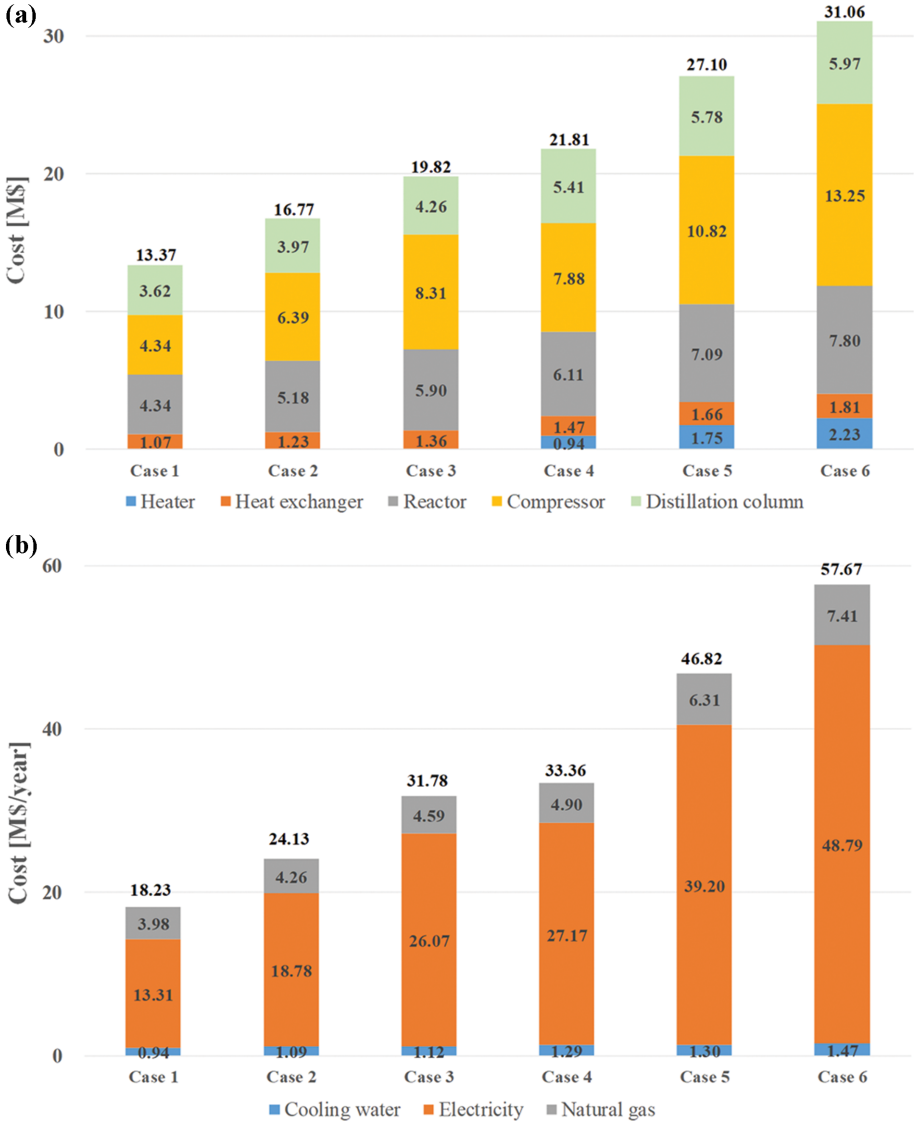

Fig. 6. (a) Purchased equipment cost and (b) operating utility cost for cases considered in the present study.

perature of the recycled stream. Differences in the costs of heat exchangers resulted from the second heat exchanger which pre-heats the stream before R2, while the operating condition for R1 was the same for all the cases. The compressor, which pressurizes the stream from 19.3 to 27 bar before COL2 for the separation of MA, was expensive and took the largest portion of the purchased equipment cost. Finally, the distillation column showed that its cost is proportional to the volume of the column to properly separate the components. Moreover, COL3 was considered only in Cases 4 to 6 to purify the inlet stream into R2, increasing the process cost. The total purchase cost of equipment in Fig. 6(a) shows that the capital investment mainly depends on the presence of the recycle loop and CO/DME ratio in R2.

Cooling water, electricity, and natural gas were considered for operating costs. Electricity took most of the utility cost as cryogenic distillation was essential on COL2 and COL3 for the separation of inert gas and MA product. In addition, the compressor before COL2 also required substantial electricity to fully pressurize the stream. It was also shown that steam was a more expensive heat source than natural gas, even though it can be more environmentally friendly. Therefore, natural gas was used as the main heat source in R2, reboilers, and heaters in the recycle loop. Compared to electricity, the cheaper price of natural gas made itself a more cost-efficient heat source (0.06 $/kWh for electricity and 0.01143 $/kWh for natural gas in Table 2). Cooling water, which took the least portion of operating cost, was used to maintain the temperature of reactors (R1, R3) and the condenser of COL1, which operated at moderate pressure above 15 °C. Total operating cost in Fig. 6(b) showed a similar tendency to capital investment cost. However, the recycle loop increased annual production by more than three-fold compared to the open-loop cases and compensated for the total production cost.

CONCLUSIONS

A process model that converts syngas into ethanol and acetic acid via the synthesis of DME and MA was developed. For DME carbonylation, a reaction rate equation was suggested based on the kinetic mechanism, and the kinetic parameters were estimated by fitting to the experimental data. The rate equations reported in our previous work were applied to the direct synthesis of DME from syngas, whereas the Gibbs-minimum reactor was used for the conversion of MA to ethanol and acetic acid. The results of the simulated process showed that the carbon molar yields in the processes with recycled streams were approximately 20 times higher than those of the open-loop processes, owing to the substantially increased levels of overall DME conversion resulting from recycling. An increase in the CO/DME ratio caused the production rate to increase at the expense of energy consumption in the separation process, which was mostly covered by the condenser duty of COL2 to separate CO. Consequently, although the production rate at the lowest CO/DME ratio was slightly lower than that at higher ratios, the lowest ratio was suggested to be the optimal case, based on the tradeoff between energy efficiency and production rate. The result of cost analysis suggested that the recycle loop increased both capital and utility costs, which was compensated by the increased production rate. In conclusion, the efficient process model developed in this study can contribute to the design of a strategy for cleaner production of valuable products using COG from steel manufacturing processes.

ACKNOWLEDGEMENT

This research was supported by the C1 Gas Refinery Program through the National Research Foundation of Korea (NRF), funded by the Ministry of Science, ICT, & Future Planning (No. NRF2021 M3D3A1A01082822, No. NRF2018M3D3A1A01018009).

NOMENCLATURE

c_i : concentration of species i [mol/m^3]
C_p : heat capacity at constant pressure [J/(kg·K)]
D_t : tube diameter [m]
E : activation energy [J/mol]
F_{obj} : objective function
ΔH : heat of reaction [J/mol]
k_j : reaction rate constant for reaction j
K_j : reaction equilibrium constant for reaction j
L : length of the reactor [m]
NE : number of experimental conditions
NR : number of reactions
R : reaction rate [mmol/(g_{cat}·h)]
u_s : gas velocity [m/s]
U : overall heat transfer coefficient [W/(m^2·K)]
T : temperature [K]
T_w : wall temperature [K]

Greek Letters

ρ_B : Bulk pellet density [kg/m^3]
ρ_g : Bulk gas density [kg/m^3]

Subscripts

calc : calculated values
exp : experimental data
i : species
in : inlet conditions
j : reactions
ref : reference

SUPPORTING INFORMATION

Additional information as noted in the text. This information is available via the Internet at http://www.springer.com/chemistry/journal/11814.

REFERENCES

1. Y. Li, S. Huang, Z. Cheng, S. Wang, Q. Ge and X. Ma, *J. Catal.*, **365**, 440 (2018).
2. H. Yue, X. Ma and J. Gong, *Acc. Chem. Res.*, **47**, 1483 (2014).
3. Y. Amao, N. Shuto and H. Iwakuni, *Appl. Catal. B.*, **180**, 403 (2016).
4. H. Zhou, W. Zhu, L. Shi, H. Liu, S. Liu, Y. Ni, Y. Liu, Y. He, S. Xu

and L. Li, *J. Mol. Catal. A, Chem.*, **417**, 1 (2016).
5. N. Zhao, Y. Tian, L. Zhang, Q. Cheng, S. Lyu, T. Ding, Z. Hu, X. Ma and X. Li, *Chin. J. Catal.*, **40**, 895 (2019).
6. X. Wang, R. Li, C. Yu, Y. Liu, L. Zhang, C. Xu and H. Zhou, *Fuel*, **239**, 794 (2019).
7. Y. Liu, K. Murata, M. Inaba and I. Takahara, *Fuel Process. Technol.*, **110**, 206 (2013).
8. H. Shen, Y. Li, S. Huang, K. Cai, Z. Cheng, J. Lv and X. Ma, *Catal. Today*, **330**, 117 (2019).
9. V. Subramani and S. K. Gangwal, *Energy Fuels*, **22**, 814 (2008).
10. N. Yoneda, S. Kusano, M. Yasui, P. Pujado and S. Wilcher, *Appl. Catal. A: Gen.*, **221**, 253 (2001).
11. P. Pal and J. Nayak, *Sep. Purif. Rev.*, **46**, 44 (2017).
12. Y. Wang, Y. Zhao, J. Lv and X. Ma, *ChemCatChem.*, **9**, 2085 (2017).
13. X. Huang, M. Ma, S. Miao, Y. Zheng, M. Chen and W. Shen, *Appl. Catal. A: Gen.*, **531**, 79 (2017).
14. F. Zhang, Z. Chen, X. Fang, H. Liu, Y. Liu and W. Zhu, *J. Energy Chem.*, **61**, 203 (2021).
15. A. Shigematsu, T. Yamada and H. Kitagawa, *J. Am. Chem. Soc.*, **134**, 13145 (2012).
16. A. Y. Pulyalina, G. A. Polotskaya, K. Y. Veremeychik, M. Y. Goikhman, I. V. Podeshvo and A. M. Toikka, *Fuel Process. Technol.*, **139**, 178 (2015).
17. Y. Dong, C. Dai and Z. Lei, *Ind. Eng. Chem.*, **57**, 11167 (2018).
18. T. Pöpken, L. Götze and J. Gmehling, *Ind. Eng. Chem.*, **39**, 2601 (2000).
19. W. Yu, K. Hidajat and A. K. Ray, *Appl. Catal. A: Gen.*, **260**, 191 (2004).
20. T. He, X. Liu, S. Xu, X. Han, X. Pan, G. Hou and X. Bao, *J. Phys. Chem. C*, **120**, 22526 (2016).
21. H. Zhan, S. Huang, Y. Li, J. Lv, S. Wang and X. Ma, *Catal. Sci. Technol.*, **5**, 4378 (2015).
22. L. Junlong, X. Huifu, X. Huang, W. Pei-Hao, S.-J. Huang, L. Shang-Bin and S. Wenjie, *Chin. J. Catal.*, **31**, 729 (2010).
23. Y. Liu, K. Murata and M. Inaba, *React. Kinet. Mech. Catal.*, **117**, 223 (2016).
24. G. J. Sunley and D. J. Watson, *Catal. Today*, **58**, 293 (2000).
25. P. Cheung, A. Bhan, G. J. Sunley, D. J. Law and E. Iglesia, *J. Catal.*, **245**, 110 (2007).
26. D. B. Rasmussen, J. M. Christensen, B. Temel, F. Studt, P. Moses, J. Rossmeisl, A. Riisager and A. D. Jensen, *Catal. Sci. Technol.*, **7**, 1141 (2017).
27. E. Zhan, Z. Xiong and W. Shen, *J. Energy Chem.*, **36**, 51 (2019).
28. J. Park, Y. Woo, H. S. Jung, H. Yang, W. B. Lee, J. W. Bae and M.-J. Park, *Catal. Today*, **388-389**, 323 (2022).
29. H. J. Jun, M.-J. Park, S.-C. Baek, J. W. Bae, K.-S. Ha and K.-W. Jun, *J. Nat. Gas Chem.*, **20**, 9 (2011).
30. N. Park, M.-J. Park, Y.-J. Lee, K.-S. Ha and K.-W. Jun, *Fuel Process. Technol.*, **125**, 139 (2014).
31. H. S. Jung, F. Zafar, X. Wang, T. X. Nguyen, C. H. Hong, Y. G. Hur, J. W. Choung, M.-J. Park and J. W. Bae, *ACS Catal.*, **11**, 14210 (2021).
32. J. M. Douglas, *Conceptual design of chemical processes*, Mc-Graw-Hill, New York (1988).
33. S. Kim, Y. Kim, S. Y. Oh, M.-J. Park and W. B. Lee, *J. Nat. Gas Sci. Eng.*, **96**, 104308 (2021).
34. R. Turton, R. C. Bailie, W. B. Whiting, J. A. Shaeiwitz and D. Bhattacharyya, *Analysis, synthesis, and design of chemical processes*, Prentice Hall, New Jersey (2018).
35. R. Bertrum Diemer and W. L. Luyben, *Ind. Eng. Chem. Res.*, **49**, 12224 (2010).
36. H. Ham, H. S. Jung, H. S. Kim, J. Kim, S. J. Cho, W. B. Lee, M.-J. Park and J. W. Bae, *ACS Catal.*, **10**, 5135 (2020).

Supporting Information

Process modeling of syngas conversion to ethanol and acetic acid via the production of dimethyl ether and its carbonylation

Seungwoo Kim*, Hyun Seung Jung, Won Bo Lee*,†, Jong Wook Bae**,†, and Myung-June Park***,****,†**

*School of Chemical and Biological Engineering, Seoul National University, Seoul 08826, Korea
**School of Chemical Engineering, Sungkyunkwan University (SKKU), Suwon 16419, Korea
***Department of Chemical Engineering, Ajou University, Suwon 16499, Korea
****Department of Energy Systems Research, Ajou University, Suwon 16499, Korea
(*Received 14 April 2022 • Revised 23 August 2022 • Accepted 15 September 2022*)

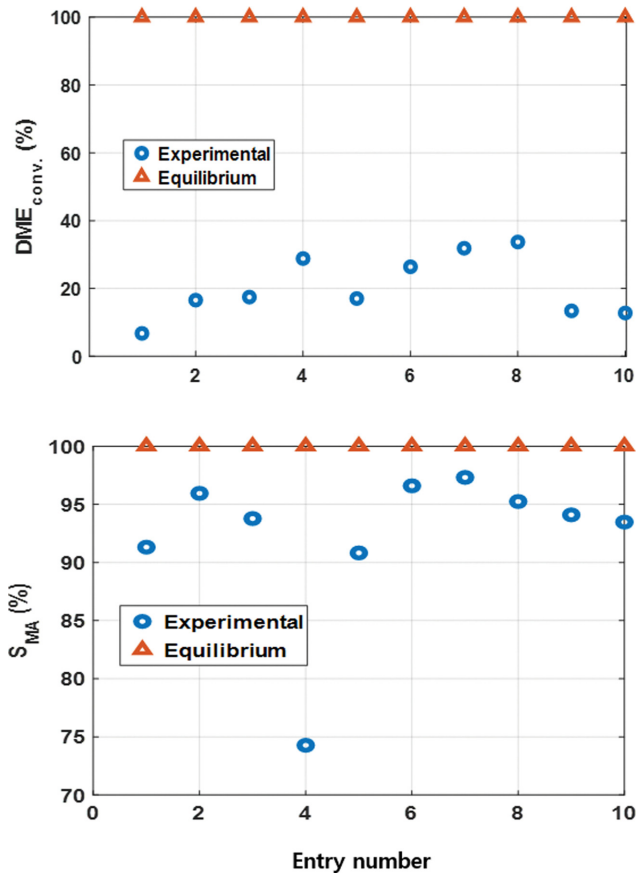

Fig. S1. Comparison among experimental and equilibrium data regarding DME carbonylation.

Reaction rate equations for direct synthesis of DME from syngas over the hybrid catalyst

CO_2 hydrogenation ($CO_2+3H_2 \leftrightarrow CH_3OH+H_2O$)

$$r_{CO_2}=\frac{k_C K_{CO_2}\left(f_{CO_2} f_{H_2}^{1.5}-\frac{f_{H_2O} f_{CH_3OH}}{K_{P,C} f_{H_2}^{1.5}}\right)}{(1+K_{CO_2} f_{CO_2})(1+K_{H_2}^{0.5} f_{H_2}^{0.5}+K_{H_2O} f_{H_2O})} \quad \text{(S1)}$$

CO hydrogenation ($CO+2H_2 \leftrightarrow CH_3OH$)

$$r_{CO}=\frac{k_A K_{CO}\left(f_{CO} f_{H_2}^{1.5}-\frac{f_{CH_3OH}}{K_{P,A} f_{H_2}^{0.5}}\right)}{(1+K_{CO} f_{CO})(1+K_{H_2}^{0.5} f_{H_2}^{0.5}+K_{H_2O} f_{H_2O})} \quad \text{(S2)}$$

Reverse water-gas-shift ($CO_2+H_2 \leftrightarrow H_2O+CO$)

$$r_{RWGS}=\frac{k_B K_{CO_2}\left(f_{CO_2} f_{H_2}-\frac{f_{CO} f_{H_2O}}{K_{P,B}}\right)}{(1+K_{CO_2} f_{CO_2})(1+K_{H_2}^{0.5} f_{H_2}^{0.5}+K_{H_2O} f_{H_2O})} \quad \text{(S3)}$$

DME synthesis ($2CH_3OH \leftrightarrow CH_3OCH_3+H_2O$)

$$r_{DME}=\frac{k_{DME} K_{CH_3OH}^2\left(C_{CH_3OH}^2-\frac{C_{H_2O} C_{DME}}{K_{P,DME}}\right)}{(1+2\sqrt{K_{CH_3OH} C_{CH_3OH}}+K_{H_2O,DME} C_{H_2O})^4} \quad \text{(S4)}$$

Here, K_i and k_i denote the adsorption equilibrium constants and the forward reaction rate constant for species *i*, respectively. Generalized correlations for the fugacity coefficient were used to calculate the fugacity (f) and the reaction equilibrium constant K_p was calculated from the process simulator (Unisim Design Suite, Honeywell Inc.).

Table S1. Energy consumption of each equipment with related utility

Utility	Equipment	Energy consumption [GJ/h]					
		Case 1	Case 2	Case 3	Case 4	Case 5	Case 6
Cooling water	R1				126.3		
	R3 (Ethanol)	11.49	15.68	18.89	38.03	39.91	40.55
	R3 (Acetic acid)	20.79	28.48	33.82	68.98	71.47	124.2
	COL1 (Condensor)				175.5		
Electricity	Compressor	15.87	25.43	35.03	32.87	48.34	62.24
	COL2 (Condensor)	70.55	115.4	160.5	147.1	221.8	279.8
	COL3 (Condensor)	-	-	-		23.89	
Natural gas	R2	15.87	26.91	40.14	13.25	37.38	62.04
	COL1 (Reboiler)				140.6		
	COL3 (Reboiler)	-	-	-		10.51	
	Heater	-	-	-	28.72	59.89	78.98